Progress In Electromagnetics Research, PIER 76, 95–126, 2007

FORWARD RADAR PROPAGATION OVER OIL SLICKS ON SEA SURFACES USING THE AMENT MODEL WITH SHADOWING EFFECT

N. Pinel, C. Bourlier, and J. Saillard

IREENA Laboratory (EA 1770) - Radar Team
Ecole Polytechnique de l'Université de Nantes
La Chantrerie, Rue C. Pauc, BP 50609, 44306 Nantes Cedex 3, France

Abstract—This paper is devoted to the forward radar propagation over clean and contaminated seas, using the Ament model and by taking the shadowing effect into account. The well-known Rayleigh parameter, which characterizes the degree of roughness of a corrugated surface for the case of reflection on a rough surface, is presented. Then, it is extended to the transmission through a rough surface, and to the reflection on a layer of two rough interfaces. This extended Rayleigh parameter allows then to calculate the forward radar propagation over oil slicks on sea surfaces, using the Ament model. Moreover, the model is improved by taking the shadowing effect into account. Numerical results of contaminated seas are presented, and compared to that of clean seas.

1. INTRODUCTION

For low grazing incidence angles, the classical asymptotic scattering models applied to natural surfaces or natural layers, like the IEM model [1–3] or the SSA model [4], are not valid any more. Thus, the Ament model [5], which is a fast and simple model that describes the forward (i.e., in the specular direction) radar propagation over rough surfaces, can be used for such a configuration. Here, based on the Parabolic Wave Equation [6–8], it is applied to the forward propagation over sea surfaces for coastal radar configuration. This model, which is based on a ray approach, uses the Rayleigh parameter to describe the scattering from the rough interface for grazing incidence in a simple way. Indeed, it takes the surface roughness into account by multiplying the Fresnel reflection coefficient of a plane surface by the term $\exp(-2R_a^2)$ (for Gaussian statistics, with R_a the Rayleigh parameter). Nevertheless, as

shown in the literature [9], this simple model enables fast results which are consistent with rigorous methods for $R_a \lesssim 1.25$ ($R_a = k_1 \sigma_h \cos\theta_i$, with σ_h the surface RMS height, k_1 the incident wave number, and θ_i the incidence angle). The model was then improved in [8] by taking the shadowing effect into account.

The interest of using this simple and efficient model is quite clear, because solving rigorously such an electromagnetic scattering problem for grazing incidence needs very long surfaces, and consequently very large computing time and memory space. Then, the extension to rough layers would be quite difficult; it is not the aim of this paper and it is then not presented here. Thus, the extension of the Ament model to the case of two rough surfaces separating homogeneous media is presented here, in order to deal with the forward propagation over rough layers. In Section 2, the Rayleigh parameter for a single rough interface is presented, with the introduction of the shadowing effect. Then, it is extended in Section 3 to the case of transmission through a rough surface and in Section 4 to the case of reflection from a rough layer. Last, it is applied in Section 5 to the forward radar propagation over a rough layer under the Ament model [10] with shadowing effect. The influence of the shadowing effect on the results is presented, for different sea states and for two frequencies $f = 3\,\text{GHz}$ and $f = 300\,\text{MHz}$.

2. AMENT MODEL FOR A SINGLE ROUGH INTERFACE

2.1. Presentation of the Ament Model

The Ament model [5] assumes that only the coherent scattered power contributes to the total scattered power. Then, under the Ament model, the power density scattered in reflection p_r from a rough surface corresponds to the *coherent* power density p_r^{coh}. The latter is given by the expression $p_r^{coh} = |\langle E_r \rangle|^2 / 2Z_1$, with Z_1 the wave impedance and E_r the field scattered in reflection inside the incident medium Ω_1. Then, for an infinite rough surface, p_r^{coh} occurs only in the specular direction (forward propagation), and differs from the one of an infinite plane surface by the multiplication of the term [10]

$$\left| \left\langle \exp(j\Delta\phi_r) \right\rangle \right|^2 = \left| \int_{-\infty}^{+\infty} \exp(j\Delta\phi_r)\, p_h(\zeta)\, d\zeta \right|^2, \tag{1}$$

where p_h is the surface height PDF (probability density function). $\Delta\phi_r$ is the phase difference between the wave scattered in reflection from a point A of the rough surface, with coordinates (x_A, ζ_A), and a point of

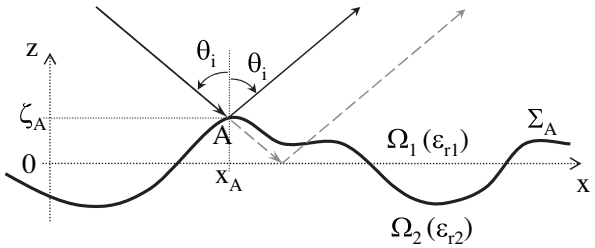

Figure 1. Degree of roughness of a random rough surface: reflection case.

the mean plane $z = 0$ (plotted in grey dashed line, see Fig. 1). It is given for a surface of infinite extent by (see Fig. 1)

$$\Delta\phi_r = 2k_1\Delta\zeta_A \cos\theta_i, \tag{2}$$

where k_1 is the wave number inside the medium Ω_1, $\Delta\zeta_A = \zeta_A$ the height deviation of point A from the mean plane $z = 0$, and θ_i the incidence angle.

For Gaussian statistics, the multiplication term in the scattered power is equal to $\exp(-4R_{a,r}^2)$, with $R_{a,r}$ the surface Rayleigh parameter. Expressed from the root mean square of $\Delta\phi_r$, it is given by the relation [11]

$$R_{a,r} = k_1\sigma_h \cos\theta_i, \tag{3}$$

with σ_h the surface RMS height.

Then, the Ament reflection coefficient r_A of the *field* scattered by the rough surface is defined as the product of the Fresnel reflection coefficient of a plane surface, r_{12} [12], with the phase variation term (equal to the characteristic function of one variable) $\langle \exp(j\Delta\phi_r)\rangle$ [5]. In what follows, we will denote the phase variation term $\langle \exp(j\Delta\phi_r)\rangle$ as $\mathcal{A}_r$. Then, the Ament reflection coefficient r_A is given by

$$r_A(\theta_i) = r_{12}(\theta_i) \times \mathcal{A}_r. \tag{4}$$

For Gaussian statistics, $\mathcal{A}_r = \exp(-2R_{a,r}^2)$ and r_A is equal to

$$r_A(\theta_i) = r_{12}(\theta_i) \times \exp(-2R_{a,r}^2). \tag{5}$$

Nevertheless, in this model the shadowing effect, which has a significant contribution for this kind of configuration (i.e., for low grazing angles), is not taken into account. This phenomenon, which was subject to a recent publication in [8], is summarized in next subsection for the case of reflection from a single interface, in order to extend it to the case of a rough layer.

2.2. Ament Model with Shadowing Effect

The classical Ament model calculates the Ament reflection coefficient using equation (4). Nevertheless, for low grazing incidence, only a part of the points of the surface are illuminated by the emitter and seen by the receiver. Then, the real height PDF (probability density function) which is concerned in equation (4) has to be modified: $p_h(\zeta)$ must be replaced by the *illuminated* height PDF $\breve{p}_{h,11}$ of the wave incident and scattered inside Ω_1. It is defined as

$$\breve{p}_{h,11}(\zeta;\theta_i) = p_h(\zeta) \times \bar{I}_{11}(\zeta,\theta_i), \tag{6}$$

where $\bar{I}_{11}$ is the associated average statistical illumination function (the first subscript refers to the incidence medium, and the second subscript refers to the scattering medium). It is defined as

$$\bar{I}_{11}(\zeta,\theta_i) = \frac{\displaystyle\int_{-\infty}^{+\infty} p_s(\gamma)\, S_{11}(\theta_i,\zeta,\gamma)\; d\gamma}{\displaystyle\int_{-\infty}^{+\infty}\int_{-\infty}^{+\infty} p_{h,s}(\zeta,\gamma)\, S_{11}(\theta_i,\zeta,\gamma)\; d\zeta d\gamma}, \tag{7}$$

where p_s is the surface slope PDF, with γ the surface slope, and $p_{h,s}$ the surface joint height and slope PDF. $S_{11}(\theta_i,\zeta,\gamma)$ is the bistatic statistical illumination function of an arbitrary point of the surface, of height ζ and slope γ, for an incidence angle θ_i.

For any uncorrelated process between the surface heights and slopes, it is given by equation (15) of [8]; for an uncorrelated Gaussian process, it is given by equations (15) and (16) of [8]; and for a correlated Gaussian process, it is given by equation (17) of [8]. Hereafter, the Smith formulation of the bistatic statistical illumination function [13, 14], denoted as $S_{11,S}(\theta_i,\zeta,\gamma)$, will be used, and we will consider uncorrelated process. In forward propagation, by considering any even process, the monostatic shadowing function associated to the incident and the scattered waves are equal, and are defined for the Smith formulation as $S_{1,S}(\theta_i,\zeta,\gamma) = [F(\zeta)]^{\Lambda(\theta_i,\sigma_s)}$. Then, in forward propagation and by considering the Smith formulation, $S_{11,S}$ is equal to

$$S_{11,S}(\theta_i,\zeta,\gamma) = \left\{[F(\zeta)]^{\Lambda(\theta_i,\sigma_s)}\right\}^2, \tag{8}$$

with $F(\zeta)$ the height cumulative function defined by

$$F(\zeta) = \int_{-\infty}^{\zeta} p_h(\zeta_0)\; d\zeta_0, \tag{9}$$

and $\Lambda(\theta_i, \sigma_s)$ is defined by

$$\Lambda(\theta_i, \sigma_s) = \frac{1}{\cot\theta_i} \int_{\cot\theta_i}^{+\infty} (\gamma - \cot\theta_i)\, p_s(\gamma)\; d\gamma, \tag{10}$$

σ_s being the surface RMS slope. Then, for an uncorrelated process between the surface heights and slopes, the average statistical illumination function $\bar{I}_{11}$ is given under the Smith formulation by

$$\bar{I}_{11,S}(\zeta, \theta_i) = [1 + 2\Lambda(\theta_i, \sigma_s)]\;\; [F(\zeta)]^{2\Lambda(\theta_i, \sigma_s)}. \tag{11}$$

Hereafter, we will consider Gaussian statistics. Then, $F(\zeta)$ is given by

$$F(\zeta) = 1 - \frac{1}{2}\,\mathrm{erfc}\Big(\frac{\zeta}{\sqrt{2}\,\sigma_h}\Big), \tag{12}$$

and $\Lambda(\theta_i, \sigma_s)$ is given by

$$\Lambda(\theta_i, \sigma_s) = \Lambda(v_i) = \frac{\exp(-v_i^2) - v_i\sqrt{\pi}\,\mathrm{erf}(v_i)}{2v_i\sqrt{\pi}}, \quad \text{with} \quad v_i = \frac{\cot\theta_i}{\sqrt{2}\,\sigma_s}. \tag{13}$$

Thus, the *illuminated* Ament reflection coefficient, $\breve{r}_A$, is defined as

$$\breve{r}_A(\theta_i) = r_{12}(\theta_i) \times \breve{\mathcal{A}}_r, \tag{14}$$

where $\breve{\mathcal{A}}_r$ is the phase variation term due to the roughness, which takes the shadowing effect into account. It differs from the term $\mathcal{A}_r$ (which does not take the shadowing effect into account) because it takes the *illuminated* height PDF into account. It is then given by

$$\breve{\mathcal{A}}_r = \int_{-\infty}^{+\infty} \exp(j\Delta\phi_r)\, \breve{p}_{h,11}(\zeta; \theta_i)\; d\zeta, \tag{15}$$

with $\breve{p}_{h,11}(\zeta; \theta_i)$ given by equation (6). Then, for an uncorrelated Gaussian process, and by considering the Smith formulation, $\breve{\mathcal{A}}_r$ is given by

$$\breve{\mathcal{A}}_r = \frac{1 + 2\Lambda_i}{\sqrt{\pi}} \int_{-\infty}^{+\infty} e^{j\sqrt{2}\sigma_h Q_r\, z - z^2} \left[1 - \frac{\mathrm{erfc}(z)}{2}\right]^{2\Lambda_i} dz, \tag{16}$$

with $\Lambda_i = \Lambda(v_i)$ and $Q_r = 2k_1 \cos\theta_i$. This integral may be computed numerically. Otherwise, as exposed in [8], and modeling $\breve{I}_{11}$ as a Gaussian PDF, an approximate expression of $\breve{\mathcal{A}}_r$ can be given

$$\breve{\mathcal{A}}_r \simeq \breve{\mathcal{A}}'_r = \exp\left(-\frac{Q_r^2 \breve{\sigma}_{h,11}^2}{2}\right) \times \exp(-jQ_r \breve{m}_{h,11}), \tag{17}$$

where $\breve{m}_{h,11}$ and $\breve{\sigma}_{h,11}$ are the mean and the RMS illuminated surface heights, respectively. Comparatively to the classical Ament reflection coefficient given by equation (5), the RMS surface height σ_h is replaced by the RMS illuminated surface height $\breve{\sigma}_{h,11}$. One can then define a new reflection Rayleigh parameter, called *illuminated* reflection Rayleigh parameter, denoted $\breve{R}_{a,r}$, and defined as

$$\breve{R}_{a,r} = k_1 \, \breve{\sigma}_{h,11} \, \cos\theta_i. \tag{18}$$

Then, $\breve{\mathcal{A}}'_r$ is given by

$$\breve{\mathcal{A}}'_r = \exp(-2\breve{R}_{a,r}^2) \times \exp(-jQ_r \breve{m}_{h,11}). \tag{19}$$

Moreover, the multiplication term $\exp(-jQ_r \breve{m}_{h,11})$ appears, which accounts for a phase deviation of the illuminated Ament reflection coefficient from the classical one: it is due to the fact that the mean illuminated surface height $\breve{m}_{h,11}$ differs from the mean surface height (which is equal to zero). For Gaussian statistics, $\breve{m}_{h,11}$ and $\breve{\sigma}_{h,11}$ can be determined using Fig. 4 of [8], or Fig. 6 hereafter.

Following the idea of Fabbro et al. [8], an intuitive approach is also proposed, where only the phase deviation $\exp(-jQ_r \breve{m}_{h,11})$ is taken into account. Then, the term $\breve{\mathcal{A}}_r$ is calculated approximately in the intuitive approach by $\breve{\mathcal{A}}''_r$, which is expressed as

$$\breve{\mathcal{A}}''_r = \mathcal{A}_r \times \exp(-jQ_r \breve{m}_{h,11}), \tag{20}$$

where $\mathcal{A}_r = \exp(-2R_{a,r}^2)$ for Gaussian statistics.

In conclusion, comparatively to the case without shadowing effect where the Ament reflection coefficient is given by equation (4), for the case with shadowing effect, the *illuminated* Ament reflection coefficient is given by equation (14), where the phase variation term $\mathcal{A}_r$ is given by equation (16). The latter can be approximated by a Gaussian fitting approximation using equation (19), or by an intuitive approach using equation (20).

After this presentation of the Ament model with shadowing effect for one rough interface, in what follows we will extend it to the

case of reflection from a layer of two rough interfaces with shadowing effect. To do so, in next section we study the Rayleigh parameter and the shadowing effect associated to the transmission through a rough interface.

3. TRANSMISSION THROUGH A ROUGH INTERFACE: RAYLEIGH PARAMETER AND SHADOWING EFFECT

In order to extend the Ament reflection coefficient to the case of a rough layer, it is necessary first to define the Rayleigh parameter associated to the transmission of the wave through a rough surface [10]. Moreover, if we take the shadowing effect into account in order to improve the model, it is necessary to define the shadowing effect associated to the transmission through the rough surface. In the first subsection, the Rayleigh parameter associated to the transmission through a rough interface [10] is recalled, and the shadowing effect for the case of transmission is presented.

3.1. Rayleigh Parameter for Transmission through the Surface

Similarly to the reflection case, the phase variation $\Delta\phi_t$ of the wave scattered in transmission, which is due to the surface roughness, is given by (see Fig. 2)

$$\Delta\phi_t = k_0 \Delta\zeta_A \left(n_1 \cos\theta_i - n_2 \cos\theta_t\right), \tag{21}$$

with k_0 the wave number in the vacuum, θ_t the transmission angle, and n_1 and n_2 the refractive indexes of media Ω_1 and Ω_2, respectively. In the specular direction of transmission, θ_t is related to θ_i by the Snell-Descartes law of a plane interface, $n_1 \sin\theta_i = n_2 \sin\theta_t$. Similarly, the

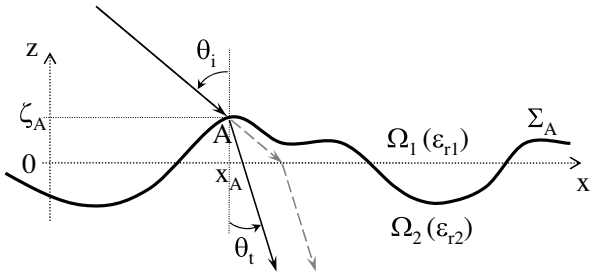

Figure 2. Degree of roughness of a random rough surface: transmission case.

Rayleigh parameter $R_{a,t}$ for the transmission case is then given by

$$R_{a,t} = k_0 \sigma_h \, \frac{|n_1 \cos\theta_i - n_2 \cos\theta_t|}{2}. \tag{22}$$

Let us note that contrary to the reflection case, where $R_{a,r}$ decreases when θ_i increases, for the transmission case, $R_{a,t}$ increases when θ_i increases. In other words, when θ_i increases, the rough surface is smoother for the reflection case and rougher for the transmission case. Then, when $\theta_i \to \pi/2$, $R_{a,r}$ tends to 0 and $R_{a,t}$ tends to

$$\lim_{\theta_i \to \pi/2} R_{a,t} = k_2 \sigma_h \, \cos\theta_t^l / 2, \tag{23}$$

with k_2 the wave number inside Ω_2, and $\theta_t^l = \arcsin(n_1/n_2)$ the limit refraction angle of a plane interface.

3.2. Shadowing Effect of Transmission through the Rough Surface

Similarly to the reflection case, the *illuminated* height PDF of a beam scattered in transmission through a rough surface, from the medium Ω_1 into the medium Ω_2, is defined as

$$\breve{p}_{h,12}(\zeta; \theta_i, \epsilon_{r2}) = p_h(\zeta) \times \bar{I}_{12}(\zeta, \theta_i, \epsilon_{r2}), \tag{24}$$

where $\bar{I}_{12}$ is the associated average statistical illumination function (the first subscript refers to the incidence medium, and the second subscript refers to the scattering medium). It is given by the relation

$$\bar{I}_{12}(\zeta, \theta_i) = \frac{\displaystyle\int_{-\infty}^{+\infty} p_s(\gamma) \, S_{12}(\theta_i, \epsilon_{r2}, \zeta, \gamma) \; d\gamma}{\displaystyle\int_{-\infty}^{+\infty} \int_{-\infty}^{+\infty} p_{h,s}(\zeta, \gamma) \, S_{12}(\theta_i, \epsilon_{r2}, \zeta, \gamma) \; d\zeta d\gamma}, \tag{25}$$

where $S_{12}(\theta_i, \epsilon_{r2}, \zeta, \gamma)$ is the bistatic statistical illumination function associated to the beam scattered in transmission through the rough surface in the specular direction.

3.2.1. Calculation of $\bar{I}_{12}$ for an Uncorrelated Process

The shadowing function devoted to the specific case of transmission through a rough interface was studied in [15]. This transmission shadowing function is obtained from two monostatic shadowing functions. The first one, $S_1(\theta_i, \zeta, \gamma)$, corresponds to the shadowing

of the surface from the incident wave of incidence angle θ_i inside Ω_1. It is given for the Smith formulation by

$$S_{1,S}(\theta_i, \zeta, \gamma) = [F(\zeta)]^{\Lambda(\theta_i, \sigma_s)}. \tag{26}$$

The second one, denoted as $S_2(\theta_t, \zeta, \gamma)$, corresponds to the masking of the surface from the scattered wave of scattering angle θ_t inside Ω_2. In forward propagation, θ_t is related to θ_i by the Snell-Descartes law $n_1 \sin\theta_i = n_2 \sin\theta_t$. $S_2(\theta_t, \zeta, \gamma)$ can then be denoted as $S_2(\theta_i, \epsilon_{r2}, \zeta, \gamma)$, and is given for the Smith formulation by the relation [15]

$$S_{2,S}(\theta_t, \zeta, \gamma) \equiv S_{2,S}(\theta_i, \epsilon_{r2}, \zeta, \gamma) = [1 - F(\zeta)]^{\Lambda(\theta_t, \sigma_s)}. \tag{27}$$

Indeed, the difference with the monostatic shadowing function inside Ω_1 is that the surface is seen from underneath. That is to say, for S_2 the wave is scattered *below* the surface inside the medium Ω_2, comparatively to S_1 where the wave is scattered *above* the surface inside the medium Ω_1. Consequently, the points of the rough surface that are concerned by the shadow are no longer $\zeta_0 \in]-\infty; \zeta]$ as in equation (26), but $\zeta_0 \in [\zeta; +\infty[$. That is why $F(\zeta)$ is transformed into $1 - F(\zeta)$.

Then, in forward propagation and by considering Gaussian statistics, the bistatic statistical shadowing function $S_{12,S}$ is equal to [15]

$$S_{12,S}(\theta_i, \epsilon_{r2}, \zeta, \gamma) = [F(\zeta)]^{\Lambda(\theta_i, \sigma_s)} [1 - F(\zeta)]^{\Lambda(\theta_t, \sigma_s)}, \tag{28}$$

where the scattering angle in transmission θ_t is related to θ_i by the Snell-Descartes law $n_1 \sin\theta_i = n_2 \sin\theta_t$. Another expression of the transmission shadowing function was previously given by Tsang and Kong in equation (2.1.156) of [16]. In the specular direction, it differs from the reflection shadowing function only by replacing the reflection angle θ_r by the transmission angle θ_t. Then, denoted as S_{12}^T, it is given for the Smith formulation by the relation

$$S_{12,S}^T(\theta_i, \epsilon_{r2}, \zeta, \gamma) = [F(\zeta)]^{\Lambda(\theta_i, \sigma_s) + \Lambda(\theta_t, \sigma_s)}. \tag{29}$$

For uncorrelated process between the surface heights and slopes, the average statistical illumination function $\bar{I}_{12}$ is given under the Smith formulation by

$$\begin{aligned} \bar{I}_{12,S}(\zeta, \theta_i) &= \left\{ B\left[1 + \Lambda(\theta_i, \sigma_s), 1 + \Lambda(\theta_t, \sigma_s)\right] \right\}^{-1} \\ &\quad \times [F(\zeta)]^{\Lambda(\theta_i, \sigma_s)} [1 - F(\zeta)]^{\Lambda(\theta_t, \sigma_s)}, \end{aligned} \tag{30}$$

where B is the beta function, also called Eulerian integral of the first kind [17]. According to Tsang and Kong [16], the average statistical illumination function $\bar{I}_{12}^{T}$ is given under the Smith formulation by

$$\bar{I}_{12,S}^{T}(\zeta,\theta_i) = [1+\Lambda(\theta_i,\sigma_s)+\Lambda(\theta_t,\sigma_s)] \times \ [F(\zeta)]^{\Lambda(\theta_i,\sigma_s)+\Lambda(\theta_t,\sigma_s)}, \quad (31)$$

Thus, the calculation of the phase variation term due to the surface roughness, $\mathcal{A}_t = \langle \exp(j\Delta\phi_t) \rangle$, is modified due to the shadowing effect. Denoted as $\breve{\mathcal{A}}_t$, it is given by

$$\breve{\mathcal{A}}_t = \int_{-\infty}^{+\infty} \exp(j\Delta\phi_t)\, \breve{p}_{h,12}(\zeta;\theta_i,\epsilon_{r2})\ d\zeta, \quad (32)$$

with $\breve{p}_{h,12}(\zeta;\theta_i,\epsilon_{r2})$ given by equation (24). Then, for an uncorrelated Gaussian process, and by considering the Smith formulation, according to the authors [15] $\breve{\mathcal{A}}_t$ is given by

$$\begin{aligned} \breve{\mathcal{A}}_t \ &= \ \frac{[B(1+\Lambda_i,1+\Lambda_t)]^{-1}}{\sqrt{\pi}} \quad (33) \\ &\times \int_{-\infty}^{+\infty} e^{j\sqrt{2}\sigma_h Q_t\, z - z^2} \left[1-\frac{\mathrm{erfc}(z)}{2}\right]^{\Lambda_i} \left[\frac{\mathrm{erfc}(z)}{2}\right]^{\Lambda_t} dz, \end{aligned}$$

with $Q_t = k_0|n_1\cos\theta_i - n_2\cos\theta_t|$. Λ_i and Λ_t denote $\Lambda(\theta_i,\sigma_s)$ and $\Lambda(\theta_i,\sigma_s)$, respectively. According to Tsang and Kong, $\breve{\mathcal{A}}_t^T$ is given by

$$\breve{\mathcal{A}}_t^T = \frac{1+\Lambda_i+\Lambda_t}{\sqrt{\pi}} \int_{-\infty}^{+\infty} e^{j\sqrt{2}\sigma_h Q_t\, z - z^2} \left[1-\frac{\mathrm{erfc}(z)}{2}\right]^{\Lambda_i+\Lambda_t} dz. \quad (34)$$

To calculate $\breve{\mathcal{A}}_t$ or $\breve{\mathcal{A}}_t^T$, the integral may be computed numerically. Otherwise, like for the reflection case, one can use an approximate expression of $\breve{\mathcal{A}}_t$. In what follows, first, the illuminated normalized height PDF $\breve{p}_{h,12}$ is studied in details, and second, the calculation of the phase variation term with shadowing effect, $\breve{\mathcal{A}}_t$, is presented using an approximate expression.

3.2.2. Illuminated Normalized Height PDF from a Monte-Carlo Method

The two approaches [15, 16] of the average statistical illumination function in transmission are compared with a Monte-Carlo method, via the calculation of the illuminated normalized height PDF $\breve{p}_{h,12}(z;\theta_i,\epsilon_{r2})$. The algorithm is based on the work of Brokelman

and Hagfors [18]. It is summarized in Table 5 of [19], in which the algorithm is extended to the general bistatic configuration. Let us briefly summarize this method. First, for a given surface height autocorrelation function, the surface heights are generated by using a spectral method. Second, for a given grazing incidence angle, if a point of the surface of index p is illuminated by the emitter, the boolean value $I_1(p) = 1$; $I_1(p) = 0$ otherwise. Third, the same way is used for the receiver, which is here located under the surface (transmission). One obtains $I_2(p)$. Thus, a point of the rough surface of index p is illuminated if it is both illuminated by the emitter and seen by the receiver: $I_{12} = (I_1 \text{ and } I_2)$. Then, the illuminated heights correspond to the indexes p for which $I_{12}(p) = 1$.

3.2.3. Numerical Results of the Illuminated Normalized Height PDF

For the Monte-Carlo method, to obtain a sufficient number of points to correctly predict the illuminated height PDF, the number of samples $N_{ech} = 20\,000 \times L_c$, with the surface autocorrelation length $L_c = 200$ units.

As in [8] for the reflection case, we represent the illuminated *normalized* height PDF $\breve{p}_{h,12}(z;\theta_i,\epsilon_{r2}) = \sqrt{2}\sigma_h\,\breve{p}_{h,12}(\zeta;\theta_i,\epsilon_{r2})$ for the transmission case (and compared to the one of the reflection case), versus the surface normalized heights $z = \zeta/(\sqrt{2}\sigma_h)$. The results will be plotted for $\theta_i = 87°$ and $\sigma_s = 0.1$. First, in order to validate the average statistical illumination function in transmission $\bar{I}_{12}$, we will first consider $\epsilon_{r2} = 1$ (the incident medium being the air, assimilated to the vacuum, then $\epsilon_{r1} = 1$). Indeed, in forward propagation, as soon as $\epsilon_{r2} \geq 1.1$, the maximum value of the transmission angle θ_t does not exceed 73°, for which the shadowing effect is negligible. Then, the results are plotted first for $\epsilon_{r2} = 1$ in Figure 3. The unshadowed normalized height PDF (denoted as 'Unshad.') is plotted in black dotted line, the illuminated normalized height PDF for the reflection case (the uncorrelated Smith formulation, denoted as 'Smith R') in red dashed line, and for the transmission case (the uncorrelated Smith formulation, denoted as 'Smith T') in dark green dash-dot line. The Monte-Carlo simulation of the transmission case (denoted as 'MC T') is plotted in green line, and the Tsang and Kong expression for the transmission case (using the uncorrelated Smith formulation, denoted as 'Tsang T') is plotted in dark green circles. In the legend, the mean value, $\breve{m}_z$ (dimensionless), and the standard deviation, $\breve{\sigma}_z$ (dimensionless) are also reported for each approach. They are defined

from $\breve{p}_h(z;\theta_i)$ as

$$\breve{m}_z = \int_{-\infty}^{+\infty} z\,\breve{p}_h(z;\theta_i)\;dz, \tag{35}$$

$$\breve{\sigma}_z = \int_{-\infty}^{+\infty} (z-\breve{m}_z)^2\,\breve{p}_h(z;\theta_i)\;dz. \tag{36}$$

One can notice that

$$\breve{m}_h = \sqrt{2}\sigma_h \times \breve{m}_z(\text{in meters}),\ \text{and}\ \breve{\sigma}_h = \sqrt{2}\sigma_h \times \breve{\sigma}_z(\text{in meters}). \tag{37}$$

In Figure 3, one can observe that the Tsang and Kong expression of the transmission illuminated normalized height PDF is equal to the Smith formulation of the reflection illuminated normalized height PDF. Indeed, as $\epsilon_{r2} = 1$ here, $\theta_t = \theta_i$, then there is no difference between both formulations. Nevertheless, this Tsang and Kong expression disagrees with the Monte-Carlo simulation: the two curves do not correspond. Especially, the mean values $\breve{m}_{z,12}$ are clearly distinct. On the contrary, the uncorrelated Smith formulation in transmission, using a new transmission shadowing function [15], is in good agreement with the Monte-Carlo simulation. The mean values $\breve{m}_{z,12}$ coincide. Let us note that the result predicted by the Smith formulation (and confirmed

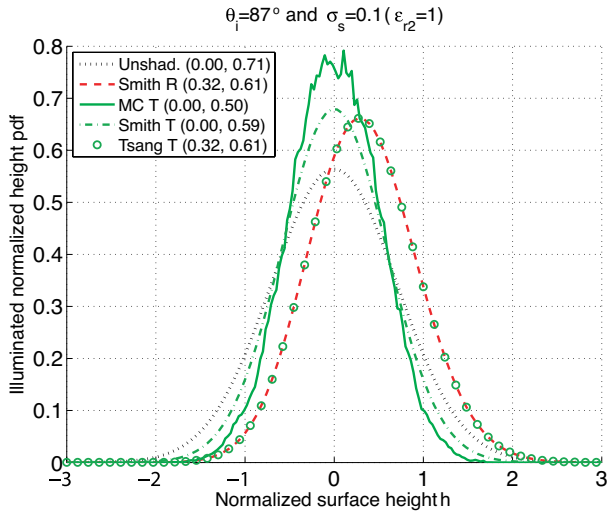

Figure 3. Illuminated normalized height PDF $\breve{p}_h(z;\theta_i,\epsilon_{r2}) = \sqrt{2}\sigma_h\,\breve{p}_h(\zeta;\theta_i,\epsilon_{r2})$ versus the surface normalized heights $z = \zeta/(\sqrt{2}\sigma_h)$ for $\theta_i = 87°$, $\sigma_s = 0.1$ and $\epsilon_{r2} = 1$.

by the Monte-Carlo simulation), $\breve{m}_{z,12} = 0$, is easily understandable. Indeed, for even surface height statistics, in the case $\epsilon_{r2} = 1$ (which leads to $\theta_t = \theta_i$), the shadowing associated to the illuminated beam equals the shadowing associated to the transmitted beam. Moreover, the two curves have similar shapes (and resemble a Gaussian PDF). One can notice though an overestimation of the standard deviation $\breve{\sigma}_{z,12}$ predicted by the uncorrelated Smith formulation with that of the Monte-Carlo simulation. This phenomenon was already observed in the reflection case, where the correlated Smith formulation allows a better prediction of the standard deviation, and a general very good agreement of the illuminated normalized height PDF. Then, it could be interesting to extend this new transmission uncorrelated Smith formulation to correlated process, for an even better prediction of the transmission illuminated normalized height PDF.

One can observe that like for the reflection case [8], the shape of the illuminated normalized height PDF for the transmission case (for both the uncorrelated Smith formulation and the Monte-Carlo simulation) resembles a Gaussian PDF. Then, for the transmission case, similarly as for the reflection case [8], an approximate expression of $\breve{p}_{h,12}$, $\breve{p}'_{h,12}$, can be given

$$\breve{p}_{h,12}(z;\theta_i) \simeq \breve{p}'_{h,12}(z;\theta_i) = \frac{1}{\breve{\sigma}_{z,12}\sqrt{2\pi}} \exp\left[-\frac{(z-\breve{m}_{z,12})^2}{2\breve{\sigma}^2_{z,12}}\right], \quad (38)$$

with $\breve{m}_{z,12}$ and $\breve{\sigma}_{z,12}$ the mean value and the standard deviation of the illuminated normalized surface heights, for the case of transmission. Figure 4 presents a comparison of the illuminated normalized height PDF $\breve{p}_h(z;\theta_i)$ (with the uncorrelated Smith formulation for reflection and transmission, and with the Monte-Carlo simulation in transmission) with a Gaussian profile versus the surface normalized heights $z = \zeta/(\sqrt{2}\sigma_h)$ for $\theta_i = 87°$ and $\sigma_s = 0.1$, with $\epsilon_{r2} = 1$. Very good agreement of the approximate expression is found with the rigorous formulation, for both reflection and transmission. Moreover, the agreement is even better for the transmission case.

Let us now have a look at the numerical results with $\epsilon_{r2} > 1$, for $\theta_i = 87°$ and $\sigma_s = 0.1$. We will take here the value $\epsilon_{r2} = 2.25$, which is a typical value of the relative permittivity of oil slicks at microwave frequencies. Nevertheless, we could take any value $\epsilon_{r2} > 1.1$, because as we wrote previously, the transmission shadowing does not contribute for this configuration, such that the results are independent of the value of $\epsilon_{r2} > 1.1$. Results are plotted in Figure 5. One can observe, as well, a good agreement of the uncorrelated Smith formulation with the Monte-Carlo simulation for the case of transmission. Numerical results

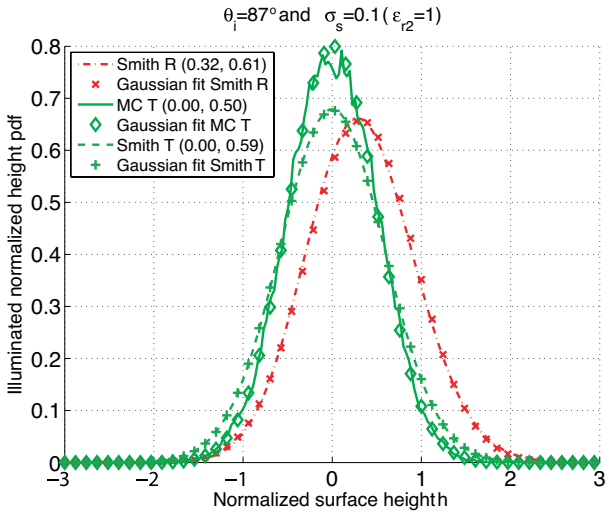

Figure 4. Comparison of the illuminated normalized height PDF $\breve{p}_h(z;\theta_i)$ with a Gaussian profile versus the surface normalized heights $z = \zeta/(\sqrt{2}\sigma_h)$ for $\theta_i = 87°$ and $\sigma_s = 0.1$.

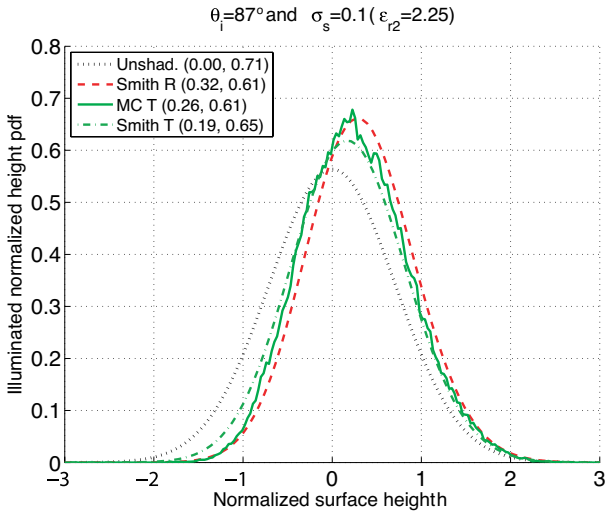

Figure 5. Illuminated normalized height PDF $\breve{p}_h(z;\theta_i,\epsilon_{r2}) = \sqrt{2}\sigma_h\,\breve{p}_h(\zeta;\theta_i,\epsilon_{r2})$ versus the surface normalized heights $z = \zeta/(\sqrt{2}\sigma_h)$ for $\theta_i = 87°$, $\sigma_s = 0.1$ and $\epsilon_{r2} = 2.25$.

confirm that the transmission shadowing does not contribute for this configuration: only the incident wave contributes to the shadowing, as other simulations (not presented here) for different values of ϵ_{r2} give exactly the same results.

Similarly as for the reflection case, in order to use equations (35) and (36), one must know the values of the mean value, $\breve{m}_{z,12}$, and the standard deviation, $\breve{\sigma}_{z,12}$, of the illuminated normalized surface heights. They are plotted in figure 6 versus the parameter of the incident wave $v_i = \cot\theta_i/(\sqrt{2}\sigma_s)$, for $\epsilon_{r2} = 1$ and $\epsilon_{r2} = 2.25$ (let us recall that for $\epsilon_{r2} > 1.1$, the results are independent of ϵ_{r2}). For $\epsilon_{r2} = 1$, one can observe that the mean value remains constant, $\breve{m}_{z,12} = 0$. As written previously, as $\theta_t = \theta_i$ here, the shadowing associated to the incident beam equals the shadowing associated to the transmitted beam. Then, the mean value remains constant and equal to zero. Likewise, as v_i decreases (corresponding to increasing θ_i), the shadowing phenomenon increases, such that the illuminated standard deviation $\breve{\sigma}_{z,12}$ decreases, and tends rapidly to 0 when v_i tends to 0. For $\epsilon_{r2} = 2.25$, the same behavior can be observed for the transmission case as for the reflection case. That is to say, for very small grazing angles or very high slope standard deviations, which corresponds to small values of v_i, the illuminated height PDF has a narrow probability distribution, and is shifted towards high heights. By contrast, when $v_i \geq 2$, $\breve{m}_h$ and $\breve{\sigma}_h$ become independent of v_i and tend to 0 and 1, respectively. Then, for $v_i \geq 2$ (which corresponds to a limit grazing incidence angle $\theta_{i,l} = \text{arccot}(2\sqrt{2}\sigma_s)$), the shadowing effect can be neglected. This corresponds, for example, for $\sigma_s = 0.1$ to $\theta_{i,l} = 74.2°$. The difference of the transmission case with the reflection case is that the mean value is a bit lower, and the standard deviation a bit higher. This is due to the fact that for the transmission case (for $\epsilon_{r2} > 1.1$), only the incident beam contributes to the shadowing effect, contrary to the reflection case where the reflected beam equally contributes to the shadowing effect (in forward propagation) as the incident beam.

3.2.4. Calculation of the Phase Variation Term with Shadowing Effect $\breve{\mathcal{A}}_t$

Similarly as for the reflection case, an approximate expression of $\breve{\mathcal{A}}_t$, $\breve{\mathcal{A}}'_t$, can be given

$$\breve{\mathcal{A}}_t \simeq \breve{\mathcal{A}}'_t = \exp\left(-\frac{Q_t^2\breve{\sigma}_{h,12}^2}{2}\right) \times \exp(-jQ_t\breve{m}_{h,12}), \qquad (39)$$

where $\breve{m}_{h,12}$ and $\breve{\sigma}_{h,12}$ are the mean and the RMS illuminated surface heights for the case of transmission, respectively. Comparatively to the classical Ament reflection coefficient, the RMS surface height σ_h is replaced by the RMS illuminated surface height $\breve{\sigma}_{h,12}$. One can then define a new transmission Rayleigh parameter, called *illuminated* transmission Rayleigh parameter, denoted as $\breve{R}_{a,t}$, and defined as

$$\breve{R}_{a,t} = k_0\, \breve{\sigma}_{h,12}\, \frac{|n_1 \cos\theta_i - n_2 \cos\theta_t|}{2}. \tag{40}$$

Then, $\breve{\mathcal{A}}'_t$ is given by

$$\breve{\mathcal{A}}'_t = \exp(-2\breve{R}^2_{a,t}) \;\times\; \exp(-jQ_t\breve{m}_{h,12}), \tag{41}$$

Moreover, the multiplication term $\exp(-jQ_t\breve{m}_{h,12})$ appears, which accounts for a phase deviation of the illuminated Ament reflection coefficient from the classical one: it is due to the fact that the mean illuminated surface height $\breve{m}_{h,12}$ differs from the mean surface height (which is equal to zero). For Gaussian statistics, $\breve{m}_{h,12}$ and $\breve{\sigma}_{h,12}$ can be determined using Fig. 6, and equation (37).

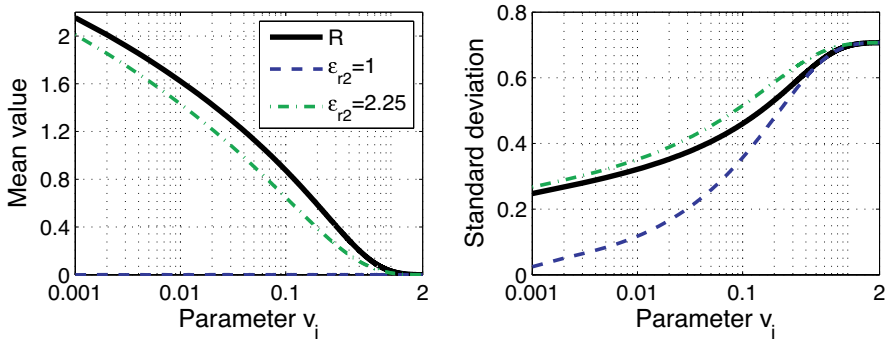

Figure 6. Mean value, $\breve{m}_z$, and standard deviation, $\breve{\sigma}_z$, of the illuminated normalized surface heights versus the parameter v_i, for the case of reflection (R) and the case of transmission for $\epsilon_{r2} = 1$ and $\epsilon_{r2} = 2.25$.

Like for the reflection case, an intuitive approach leads to the following approximation of $\breve{\mathcal{A}}_t$, denoted as $\breve{\mathcal{A}}''_t$

$$\breve{\mathcal{A}}''_t = \mathcal{A}_t \;\times\; \exp(-jQ_t\breve{m}_{h,12}), \tag{42}$$

After a detailed analysis of the specific case of transmission through a rough interface and its associated Rayleigh parameter,

illuminated height PDF, and phase variation term, let us focus now on the main goal of the paper. That is to say, the extension of the Ament model to a layer of two rough interfaces, by taking the shadowing effect into account.

4. AMENT MODEL EXTENDED TO A ROUGH LAYER WITH SHADOWING EFFECT

4.1. Rayleigh Parameters Associated to the Reflection from the Rough Layer

For the case of a rough layer (see Fig. 7), the incident wave undergoes multiple successive reflections inside Ω_2, which induce an infinite number n of reflected fields inside Ω_1, $E_1, E_2 \dots E_n$. Then, a Rayleigh parameter $R_{a,1}, R_{a,2} \dots R_{a,n}$ (and a phase variation term $\mathcal{A}_1, \mathcal{A}_2 \dots \mathcal{A}_n$) can be associated to the phase variations $\Delta\phi_1, \Delta\phi_2 \dots \Delta\phi_n$ of each scattered wave $E_1, E_2 \dots E_n$, respectively. For the first-order reflected field E_1, $\Delta\phi_1$ corresponds to the phase difference defined by equation (2):

$$\Delta\phi_1 = k_1 \Delta\zeta_{A_1} \cos\theta_i. \tag{43}$$

For the second-order reflected field E_2 (see Fig. 7), $\Delta\phi_2$ is calculated using the same way. It results from the scattering in transmission through the upper interface Σ_A, the scattering in reflection from the lower interface Σ_B, and then the scattering in

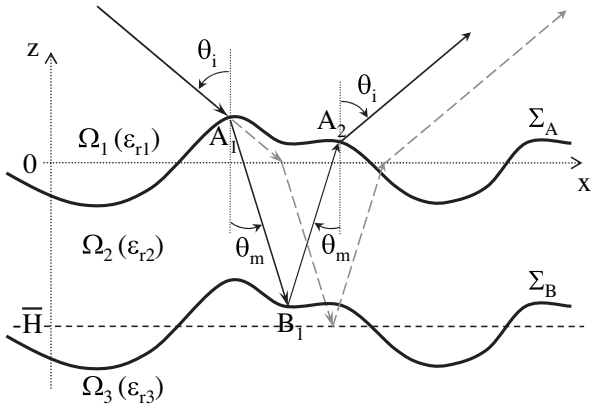

Figure 7. Degree of roughness of a random rough layer: 2nd-order contribution.

transmission through Σ_A back into the incident medium Ω_1. Thus, it is given by the expression

$$\begin{aligned}\Delta\phi_2 = \; & k_0\Delta\zeta_{A_1}\,(n_1\cos\theta_i - n_2\cos\theta_m) + 2k_2\Delta\zeta_{B_1}\,\cos\theta_m \\ & +k_0\Delta\zeta_{A_2}\,(n_1\cos\theta_i - n_2\cos\theta_m),\end{aligned} \tag{44}$$

where $\Delta\zeta_{B_1} = \zeta_{B_1} + \bar{H}$ is the height deviation from the mean plane $z = -\bar{H}$ of the lower surface. Using the same way, the phase deviation $\Delta\phi_3$ of the third-order reflected field E_3 is given by

$$\begin{aligned}\Delta\phi_3 = \; & k_0(\Delta\zeta_{A_1} + \Delta\zeta_{A_3})\,(n_1\cos\theta_i - n_2\cos\theta_m) \\ & +2k_2(\Delta\zeta_{B_1} - \Delta\zeta_{A_2} + \Delta\zeta_{B_2})\,\cos\theta_m.\end{aligned} \tag{45}$$

Similarly, $\Delta\phi_4$ of the fourth-order reflected field E_4 is given by

$$\begin{aligned}\Delta\phi_4 = \; & k_0(\Delta\zeta_{A_1} + \Delta\zeta_{A_4})\,(n_1\cos\theta_i - n_2\cos\theta_m) \\ & +2k_2(\Delta\zeta_{B_1} - \Delta\zeta_{A_2} + \Delta\zeta_{B_2} - \Delta\zeta_{A_3} + \Delta\zeta_{B_3})\cos\theta_m,\end{aligned} \tag{46}$$

and so on for the higher orders.

Then, the first-order Rayleigh parameter $R_{a,1}$ associated to E_1 is given by equation (3) using $\sigma_h \equiv \sigma_{hA}$ the RMS height of the upper surface. Similarly, the phase variation term $\mathcal{A}_1 = \left\langle e^{j\Delta\phi_1}\right\rangle$ is given by equation (4). For uncorrelated surface points, the second-order Rayleigh parameter $R_{a,2}$ associated to E_2 is given by

$$R_{a,2}^2 = 2R_{a,t12}^2 + R_{a,r23}^2, \tag{47}$$

with $R_{a,t12}$ given by equation (22) using $\sigma_h \equiv \sigma_{hA}$, and $R_{a,r23}$ by

$$R_{a,r23} = k_2\sigma_{hB}\,\cos\theta_m, \tag{48}$$

with $\sigma_h \equiv \sigma_{hB}$ the RMS height of the lower surface. Then, the phase variation term $\mathcal{A}_2 = \left\langle e^{j\Delta\phi_2}\right\rangle$ term can be split up into elementary phase variation terms such that

$$\mathcal{A}_2 = \mathcal{A}_{t12}\;\mathcal{A}_{r23}\;\mathcal{A}_{t21}, \tag{49}$$

with

$$\mathcal{A}_{t12} = \left\langle e^{j\,k_0(n_1\cos\theta_i - n_2\cos\theta_m)\,\Delta\zeta_{A_1}}\right\rangle, \tag{50a}$$

$$\mathcal{A}_{r23} = \left\langle e^{j\,2k_2\cos\theta_m\,\Delta\zeta_{B_1}}\right\rangle, \tag{50b}$$

$$\mathcal{A}_{t21} = \left\langle e^{j\,k_0(n_1\cos\theta_i - n_2\cos\theta_m)\,\Delta\zeta_{A_2}}\right\rangle. \tag{50c}$$

In the notations of the elementary phase terms, the first subscript ('r' or 't') refers to reflection or transmission, respectively, the second subscript refers to the incidence medium, and the third subscript refers to the scattering medium. In what follows, we suppose that both surfaces obey a stationary process, then $\mathcal{A}_{t21} = \mathcal{A}_{t12}$.

The expressions of the Rayleigh parameters and the phase variation terms can easily be generalized to any order $n \geq 2$. $R_{a,n}$ is given by

$$R_{a,n}^2 = 2R_{a,t12}^2 + (n-1)R_{a,r23}^2 + (n-2)R_{a,r21}^2, \tag{51}$$

with

$$R_{a,r21} = k_2 \sigma_{hA} \cos\theta_m. \tag{52}$$

Then, the phase variation term $\mathcal{A}_n = \left\langle e^{j\Delta\phi_n} \right\rangle$ is given by

$$\mathcal{A}_n = \mathcal{A}_{t12}^2 \ \mathcal{A}_{r23}^{n-1} \ \mathcal{A}_{r21}^{n-2}, \tag{53}$$

with

$$\mathcal{A}_{r21} = \left\langle e^{j\,2k_2 \cos\theta_m \,\Delta\zeta_{A_k}} \right\rangle, \tag{54}$$

where $k \in \{1 \ldots n\}$ (for a stationary process of the upper surface).

4.2. Application to the Ament Equivalent Reflection Coefficient of a Rough Layer

For the case of a layer of plane interfaces, the equivalent reflection coefficient r^{eq} [12] can be written in the form

$$r^{eq}(\theta_i) = r_{12}(\theta_i) + t_{12}(\theta_i)t_{21}(\theta_m) \sum_{k=0}^{\infty} {r_{23}}^{k+1}(\theta_m){r_{21}}^{k}(\theta_m) e^{-j(k+1)\phi_{pl}}, \tag{55}$$

with r_{ij} and t_{ij} the Fresnel reflection and transmission coefficients from the medium Ω_i to the medium Ω_j, respectively, and $\phi_{pl} = 2k_2\bar{H}\cos\theta_m$ the phase difference between E_1 and E_2. Owing to the roughness of both interfaces, one can define the Ament equivalent reflection coefficient r_A^{eq} as

$$\begin{aligned} r_A^{eq}(\theta_i) = r_{12}(\theta_i)\mathcal{A}_1 \ + \ & t_{12}(\theta_i)t_{21}(\theta_m) \\ & \times \sum_{k=0}^{\infty} {r_{23}}^{k+1}(\theta_m){r_{21}}^{k}(\theta_m) e^{-j(k+1)\phi_{pl}} \mathcal{A}_{k+2}, \end{aligned} \tag{56}$$

with $\mathcal{A}_1 = \left\langle e^{j\Delta\phi_1} \right\rangle$ (equal to $\mathcal{A}_r$ from equation (4)) and $\mathcal{A}_{k+2} = \left\langle e^{j\Delta\phi_{k+2}} \right\rangle$. For uncorrelated surface points, the latter equation can be simplified. Comparatively to the plane case where r^{eq} can be written as

$$r^{eq}(\theta_i) = r_{12}(\theta_i) + \frac{t_{12}(\theta_i)t_{12}(\theta_m)C}{1 - r_{21}(\theta_m)C}, \tag{57}$$

with $C = r_{23}(\theta_m)e^{-j\phi_{pl}}$, $r_A^{eq}(\theta_i)$ can be expressed as

$$r_A^{eq}(\theta_i) = r_{12}(\theta_i)\,\mathcal{A}_1 + \frac{t_{12}(\theta_i)t_{21}(\theta_m)C\,\mathcal{A}_2}{1 - r_{21}(\theta_m)C\,\mathcal{A}_{r21}\mathcal{A}_{r23}}, \tag{58}$$

where the first term of the right-hand side of the equation, $r_{12}(\theta_i)\,\mathcal{A}_1$, gives the Ament reflection coefficient of the upper interface. For Gaussian statistics, the phase variation terms are given by $\mathcal{A}_1 = e^{-2R_{a,1}^2}$, $\mathcal{A}_2 = e^{-2R_{a,2}^2}$, $\mathcal{A}_{r21} = e^{-2R_{a,r21}^2}$, and $\mathcal{A}_{r23} = e^{-2R_{a,r23}^2}$.

4.3. Shadowing Effect of Reflection from the Rough Layer

Like previously, taking the shadowing effect into account implies the modification of the phase variation terms $\mathcal{A}_k = \left\langle e^{j\Delta\phi_k} \right\rangle$, which are then denoted $\breve{\mathcal{A}}_k$. As a consequence, the *illuminated* Ament equivalent reflection coefficient $\breve{r}_A^{eq}$ is given by

$$\begin{aligned}\breve{r}_A^{eq}(\theta_i) = r_{12}(\theta_i)\breve{\mathcal{A}}_1 \;+\; & t_{12}(\theta_i)t_{21}(\theta_m) \\ & \times \sum_{k=0}^{\infty} {r_{23}}^{k+1}(\theta_m){r_{21}}^{k}(\theta_m)e^{-j(k+1)\phi_{pl}}\breve{\mathcal{A}}_{k+2},\end{aligned} \tag{59}$$

which can be simplified as

$$\breve{r}_A^{eq}(\theta_i) = r_{12}(\theta_i)\,\breve{\mathcal{A}}_1 + \frac{t_{12}(\theta_i)t_{21}(\theta_m)C\,\breve{\mathcal{A}}_2}{1 - r_{21}(\theta_m)C\,\breve{\mathcal{A}}_{r21}\breve{\mathcal{A}}_{r23}}. \tag{60}$$

In the calculations of the phase variation terms with shadowing effect $\breve{\mathcal{A}}_k$, for $k = 1$, $\breve{\mathcal{A}}_1$ was studied in details in subsection 2.2. For $k = 2$, $\breve{\mathcal{A}}_2$ is given by the relation

$$\breve{\mathcal{A}}_2 = \breve{\mathcal{A}}_{t12}^2\;\breve{\mathcal{A}}_{r23}, \tag{61}$$

and for $k \geq 3$, $\breve{\mathcal{A}}_k$ is given by the relation

$$\breve{\mathcal{A}}_k = \breve{\mathcal{A}}_{t12}^2\;\breve{\mathcal{A}}_{r23}^{k-1}\;\breve{\mathcal{A}}_{r21}^{k-2}. \tag{62}$$

The elementary phase variation term $\breve{\mathcal{A}}_{t12}$ is detailed in subsection 3.2, where $\zeta \equiv \zeta_A$ is the height of the upper surface Σ_A.

The term $\breve{\mathcal{A}}_{r23}$ differs from $\breve{\mathcal{A}}_1$ in the fact that the considered surface height ζ does not concern the upper surface Σ_A, but the lower surface Σ_B, and that the reflection occurs inside the medium Ω_2 onto the lower surface Σ_B, with an incidence angle θ_m. For example, the illuminated height PDF $\breve{p}_{h,11}(\zeta = \zeta_A; \theta_i)$ is replaced by $\breve{p}_{h,22}(\zeta = \zeta_B; \theta_m)$; then, θ_i is replaced by θ_m, ζ_A by ζ_B, and the subscript 1 by the subscript 2.

The term $\breve{\mathcal{A}}_{r21}$ differs from $\breve{\mathcal{A}}_1$ in the fact that the reflection onto the upper interface Σ_A does not occur above the surface inside the medium Ω_1, but below the surface inside the medium Ω_2. Moreover, the incidence angle θ_i is replaced by θ_m. Then, the illuminated height PDF $\breve{p}_{h,11}(\zeta_A; \theta_i)$ is replaced by $\breve{p}_{h,22}(\zeta_A; \theta_m)$. Its calculation must be expressed here, as it differs from $\breve{p}_{h,11}(\zeta_A; \theta_i)$ and $\breve{p}_{h,12}(\zeta_A; \theta_i)$. It is defined as

$$\breve{p}_{h,22}(\zeta_A; \theta_m) = p_h(\zeta_A) \times \bar{I}_{22}(\zeta_A, \theta_m), \tag{63}$$

where $\bar{I}_{22}$ is the associated average statistical illumination function, given by the relation

$$\bar{I}_{22}(\zeta_A, \theta_m) = \frac{\displaystyle\int_{-\infty}^{+\infty} p_s(\gamma_A)\, S_{22}(\theta_m, \zeta_A, \gamma_A)\; d\gamma_A}{\displaystyle\int_{-\infty}^{+\infty} \int_{-\infty}^{+\infty} p_{h,s}(\zeta_A, \gamma_A)\, S_{22}(\theta_m, \zeta_A, \gamma_A)\; d\zeta_A d\gamma_A}, \tag{64}$$

where p_s is the upper surface slope PDF, with γ_A the upper surface slope, and $p_{h,s}$ the upper surface joint height and slope PDF. $S_{22}(\theta_m, \zeta_A, \gamma_A)$ is the bistatic statistical illumination function of an arbitrary point of the upper surface, of height ζ_A and slope γ_A, for an incidence angle θ_m.

Here, the Smith formulation of the bistatic statistical illumination function [13, 14], denoted as $S_{22,S}(\theta_m, \zeta_A, \gamma_A)$, is used, and only uncorrelated process is considered. In forward propagation, by considering any even autocorrelation function, the monostatic shadowing function associated to the incident and the scattered waves are equal, and are defined for the Smith formulation as $S_2(\theta_m, \zeta_A, \gamma_A) = [1 - F(\zeta_A)]^{\Lambda(\theta_m, \sigma_{sA})}$. Then, in forward propagation and by considering the Smith formulation, $S_{22,S}$ is equal to

$$S_{11,S}(\theta_i, \zeta, \gamma) = \left\{ [1 - F(\zeta_A)]^{\Lambda(\theta_m, \sigma_{sA})} \right\}^2, \tag{65}$$

σ_{sA} being the upper surface RMS slope. Then, for an uncorrelated process between the surface heights and slopes, the average statistical illumination function $\bar{I}_{22}$ is given under the Smith formulation by

$$\bar{I}_{22,S}(\zeta_A, \theta_m) = [1 + 2\Lambda(\theta_m, \sigma_{sA})] \ [1 - F(\zeta_A)]^{2\Lambda(\theta_m, \sigma_{sA})}. \tag{66}$$

Hereafter, we will consider Gaussian statistics. Then, $F(\zeta_A)$ is given by

$$F(\zeta_A) = 1 - \frac{1}{2}\operatorname{erfc}\Big(\frac{\zeta_A}{\sqrt{2}\,\sigma_{hA}}\Big), \tag{67}$$

where $\Lambda(\theta_m, \sigma_{sA})$ is defined by

$$\Lambda(\theta_m, \sigma_{sA}) \equiv \Lambda(v_m) = \frac{\exp(-v_m^2) - v_m\sqrt{\pi}\,\operatorname{erf}(v_m)}{2v_m\sqrt{\pi}}, \tag{68}$$

with $v_m = \cot\theta_m/\sqrt{2}\,\sigma_{sA}$.

Then, in what follows this new Ament model for rough layers with shadowing effect is applied to the detection of oil slicks on sea surfaces.

5. APPLICATION TO FORWARD RADAR PROPAGATION OVER OIL SLICKS ON SEA SURFACES

This new Ament equivalent reflection coefficient is applied to the forward radar propagation over sea surfaces covered in oil (called contaminated seas) and compared to clean sea surfaces. That is to say, for clean sea surfaces, one will use equation (4) for the case without shadowing effect, and equation (14) for the case with shadowing effect. For contaminated seas, one will use equation (58) for the case without shadowing effect, and equation (60) for the case with shadowing effect.

Then, the considered Ament reflection coefficient (which we will denote r in general) is applied to the propagation factor η, which is used to quantify the forward propagation above clean or contaminated seas. η is defined as the ratio of the field strength at the receiver reflected by the rough (clean or contaminated) sea divided by the field strength at the receiver if it were in free space (denoted as "direct field", see Fig. 8). Then, the propagation factor η is given by the relation [9]

$$\eta = \sqrt{1 + |r|^2 + 2|r|\cos(k_1\delta + \angle r)}, \tag{69}$$

with $|r|$ and $\angle r$ the modulus and the phase of the considered Ament reflection coefficient, respectively, k_1 the incident wave number, and

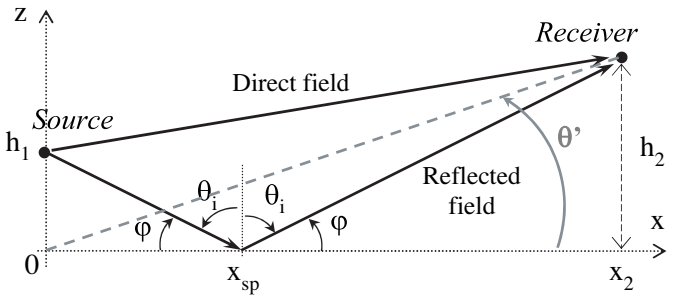

Figure 8. Forward propagation over rough surfaces: configuration.

δ the path difference between the direct and reflected fields, which is given by

$$\delta = \frac{h_1 + h_2}{\sin\varphi} - \sqrt{(h_2 - h_1)^2 + {x_2}^2}. \tag{70}$$

h_1 and h_2 denote the heights of the source and the receiver, respectively, separated by a horizontal distance x_2 (the source being located above the origin, $x_1 = 0$). $\varphi = \pi/2 - \theta_i$ is the grazing angle (see Fig. 8), given by the relation $\tan\varphi = (h_1 + h_2)/x_2$.

The calculations are performed at a frequency of 3 GHz ($\lambda = 0.1\,\mathrm{m}$), and then 300 MHz ($\lambda = 1\,\mathrm{m}$) for a horizontally ($H$) polarized radar source (and then also for vertical, V, polarization). The complex relative permittivities of oil and seawater are given at 3 GHz by [20, 21, 9]

$$\underline{\epsilon}_{r2} \simeq 2.2 + j\,0.01, \tag{71}$$
$$\underline{\epsilon}_{r3} \simeq 70 + j\,41, \tag{72}$$

respectively, and at 300 MHz by [20, 21]

$$\underline{\epsilon}_{r2} \simeq 2.25 + j\,0.01, \tag{73}$$
$$\underline{\epsilon}_{r3} \simeq 75 + j\,250, \tag{74}$$

respectively. The radar source is located at a fixed height $h_1 = 15\,\mathrm{m}$ above the origin ($x_1 = 0$). The target or receiver is at an arbitrary altitude h_2, and is located at a range $x_2 = 2\,\mathrm{km}$ away from the source (see Fig. 8). The calculations are led first for a wind speed at 10 m over the surface $u_{10} = 7\,\mathrm{m/s}$. Then, using the Elfouhaily *et al.* sea height spectrum [22], the sea surface RMS height equals $\sigma_h^{sea} \simeq 0.32\,\mathrm{m}$. For a sea covered in oil, the height spectrum is modified by the oil slick. The Lombardini *et al.* height spectrum [23] is used here for a sea covered in

oil, which depends on the characteristic pulsation ω_D and the elasticity modulus E_0 of the oil film. This model is independent of the oil layer thickness, and is valid for oil thicknesses of the order of a hundred micrometers to a millimeter. For more details, see [24]. In what follows, we consider a sea covered by an insoluble film of characteristic pulsation $\omega_D = 6$ rad/s and a elasticity modulus $E_0 = 9\,\mathrm{mN/m}$ for the oil slick. Then, for $u_{10} = 7$ m/s, the RMS surface heights of both interfaces (i.e., air-oil and oil-sea interfaces) equal $\sigma_{hA} = \sigma_{hB} \simeq 0.29$ m. Moreover, the RMS slope of the clean and contaminated seas are [25] $\sigma_h^{sea} \simeq 0.156$ and $\sigma_{hA} = \sigma_{hB} \simeq 0.105$, respectively.

5.1. Influence of the Method Used

The numerical results present a comparison between a clean sea surface and a sea covered in oil, for a frequency $f = 3\,\mathrm{GHz}$ and a wind speed $u_{10} = 7\,\mathrm{m/s}$. Fig. 9 presents the propagation factor η in dB with respect to the height of the receiver h_2, for a range $x_2 = 2\,\mathrm{km}$. One studies here the influence of the shadowing effect in general, and the influence of the method used to quantify the shadowing effect in

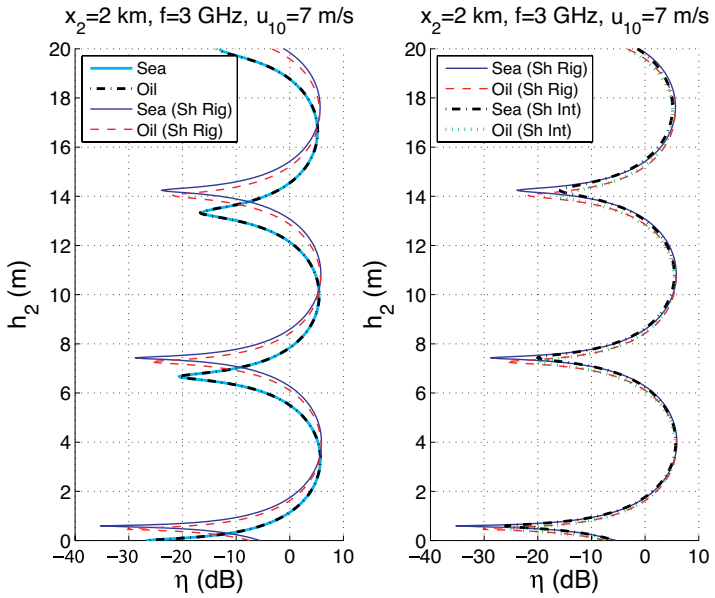

Figure 9. Numerical results of a clean sea surface and a sea covered in oil for H polarization, with $f = 3\,\mathrm{GHz}$, $x_2 = 2\,\mathrm{km}$, and $u_{10} = 7\,\mathrm{m/s}$: Comparison of the methods used.

particular. That is to say, one compares the rigorous approach (under the uncorrelated Smith formulation, given by equation (16) for the clean sea surface) with the Gaussian fitting (given by equation (19) for the clean sea surface) and the intuitive approach (given by equation (20) for the clean sea surface). In what follows, the rigorous approach is represented in the legends of the figures by "Sh Rig", the Gaussian fitting approximation by "Sh Gauss", and the intuitive approach by "Sh Int". The clean sea surface is denoted as "Sea", and for the sea covered in oil, the contribution of the upper oil surface is denoted as "Oil"and the total contribution as "Oil+Sea".

In Fig. 9, on the left, the clean sea surface is compared to the contribution of the upper oil surface of the sea covered in oil. Figures are plotted for the case without shadowing effect as well as for the rigorous approach of the shadowing effect. On the right, the intuitive approach is compared to the rigorous approach of the shadowing effect.

First, one can observe that contrary to the case without shadowing effect where the difference between the sea and the oil is quite weak, for the case with shadow, the detection of the oil is possible. Indeed, the two curves have different values and positions of minima. Moreover, comparing the three approaches of the shadowing effect, like for the clean sea surface [8], for the oil surface, there is no significant difference between the Gaussian fitting approximation and the rigorous formulation (the Gaussian fitting approximation is not represented here). On the contrary, the intuitive approach highlights a noticeable difference with the rigorous formulation. The positions of the extrema are identical, as the phase correction term $\exp(-jQ_r\breve{m}_{h,12})$ appears both in the Gaussian approximation and the intuitive approach. The lower dynamics of the curve of the intuitive approach is due to the fact that this approach considers the real surface RMS height σ_h, contrary to the Gaussian or the rigorous approaches that take the illuminated surface RMS height $\breve{\sigma}_{h,12} < \sigma_h$.

In what follows, the intuitive and the rigorous approaches will be retained in the numerical results to describe the surface shadowing effect.

5.2. Comparison for Different Configurations

The propagation factor η is plotted in Fig. 10 with respect to the height of the receiver h_2, and is compared between a clean sea surface and a sea covered in oil, for $f = 3\,\text{GHz}$ and $u_{10} = 7\,\text{m/s}$: on the left, $x_2 = 2\,\text{km}$, and on the right, $x_2 = 5\,\text{km}$. For $x_2 = 2\,\text{km}$, h_2 ranges from 0 to 30 m, which implies that the reflection Rayleigh parameter $R_{a,r}$ ranges from 0.151 to 0.453, which is in the validity domain of the

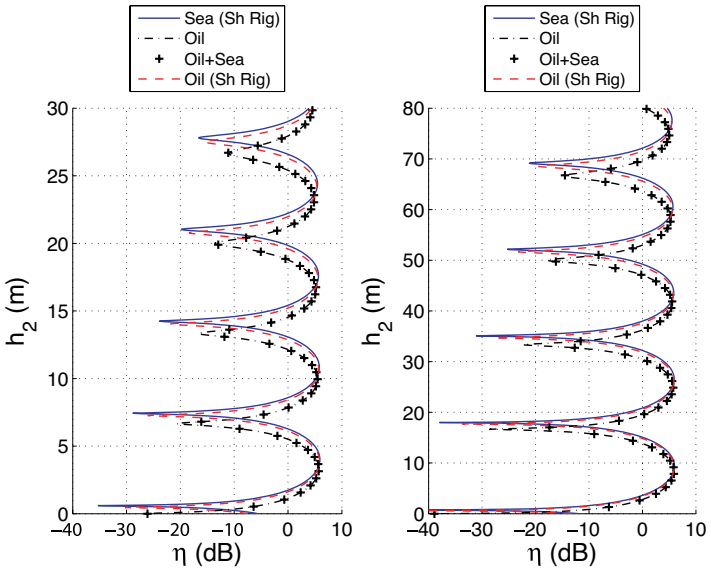

Figure 10. Comparison between a clean sea surface and a sea covered in oil with shadowing effect for H polarization, with $f = 3\,\text{GHz}$ and $u_{10} = 7\,\text{m/s}$: on the left, $x_2 = 2\,\text{km}$, and on the right, $x_2 = 5\,\text{km}$.

Ament model ($R_{a,r} < 1.25$ [9]). Likewise, for $x_2 = 5\,\text{km}$, h_2 ranges from 0 to 80 m, which implies that $R_{a,r}$ ranges from 0.060 to 0.382.

First, one can notice that the differences between the first-order of the Ament equivalent reflection coefficient, $r_{12}\,\mathcal{A}_1$ (corresponding to the reflection from the air/oil interface) and the total Ament equivalent reflection coefficient r_A^{eq}, are negligible without shadowing effect. The same conclusion can be drawn with shadowing effect (not represented here). This implies that for this configuration, only the first-order of r_A^{eq} (or $\breve{r}_A^{eq}$) contributes to η. Indeed, with $h_2 \in [0;30]$ m for $x_2 = 2$ km and $h_2 \in [0;80]$ m for $x_2 = 5$ km, the incidence angle $\theta_i > 88.6°$ for $x_2 = 2$ km and $\theta_i > 88.9°$ for $x_2 = 5$ km. Then, the reflection Rayleigh parameter $R_{a,r}^2 \approx 0$ leading to $0.639 < e^{-2R_{a,1}^2} < 0.993$, but the second-order Rayleigh parameter $R_{a,2}^2 > 585$, leading to $e^{-2R_{a,2}^2} = 0$. Thus, only the first order of r_A^{eq} contributes to η, and it would be necessary to work at much lower frequencies so that the orders 2 and more can contribute to η. The same conclusion can be drawn for the case with shadowing effect. Then, for the typical applications presented here, the sea covered in oil can be taken into account by considering only the (upper) oil surface.

As observed in Fig. 9 and in a recent article [10] for the case without shadowing effect, the differences between the clean sea surface and the sea covered in oil are slight, and are significant only around the minima or the maxima of the propagation factor η. The differences can be attributed to the differences in the RMS surface heights, as well as the values of the Fresnel reflection coefficient $r_{12}(\theta_i)$, which differ owing to the contrast of the relative permittivities of the two media. Nevertheless, this contrast is low for this range of heights h_2, corresponding to low grazing angles θ' (see Fig. 8): indeed, θ' ranges from 0° to 1°, which implies for $x_2 = 2$ km that θ_i ranges from 89.6° to 88.6°. Then, for very high θ_i, $|r_{12}(\theta_i)| \approx 1$, and the contrast increases when θ_i decreases (corresponding to increasing θ', or increasing h_2), as it can be seen in Fig. 9. This also means that the contrast increases for a lower range $x_2 < 2$ km: the detection of the oil slick is easier for low to moderate ranges x_2. As well, for higher heights h_2 of the receiver, corresponding to higher values of θ', this contrast increases.

For the case with shadowing effect, as already observed in Fig. 9, the differences between the clean sea surface and the sea covered in oil are significant owing to the phase difference between the two curves. Then, the positions of the extrema are different, and one can observe a significant difference in the values of the minima (and a slight difference in the positions of the minima). This makes it possible to detect oil slicks more easily. Nevertheless, for small heights, this difference is weak, which implies for this frequency range to work at quite high heights h_2.

In what follows, simulations are presented for a lower frequency $f = 300$ MHz, for H polarization as well as for V polarization.

5.3. Extension to V Polarization

Fig. 11 presents the propagation factor η in dB with respect to h_2 for both H and V polarizations, with a wind speed $u_{10} = 10$ m/s and a frequency $f = 3$ GHz. For V polarization, like for H polarization, only the first-order of r_A^{eq} contributes to η for this configuration (it is not presented here). For a wind speed $u_{10} = 10$ m/s, the RMS height of the clean sea surface is $\sigma_h^{sea} \simeq 0.659$ m, and the ones for the contaminated sea are $\sigma_{hA} = \sigma_{hB} \simeq 0.616$ m. As well, the RMS slope of the clean sea surface is $\sigma_s^{sea} \simeq 0.186$, and the ones for the contaminated sea are $\sigma_{sA} = \sigma_{sB} \simeq 0.116$. Then, for $x_2 = 2$ km, h_2 ranges from 0 to 30 m, which implies that $R_{a,r}$ ranges from 0.310 to 0.931, which is in the validity domain of the Ament model [9]. Likewise, for $x_2 = 5$ km, h_2 ranges from 0 to 80 m, which implies that $R_{a,r}$ ranges from 0.124 to 0.786.

For H polarization, as in the preceding configuration, the

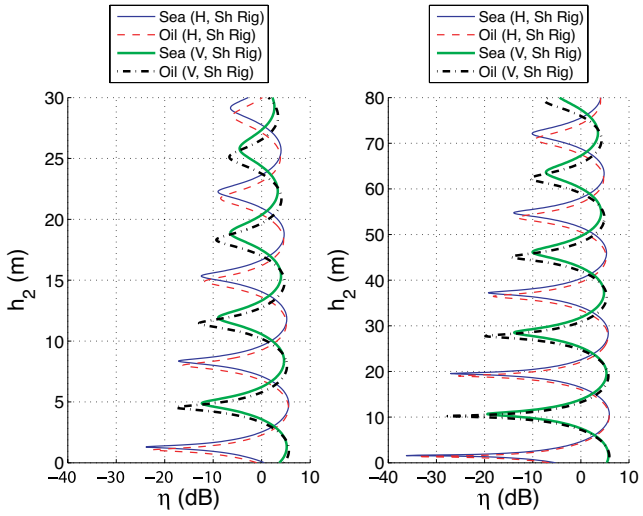

Figure 11. Comparison between a clean sea surface and a sea covered in oil for H and V polarizations, with $u_{10} = 10$ m/s and $f = 3\,\mathrm{GHz}$.

differences between the clean sea surface and the sea covered in oil are significant around the extrema of the propagation factor η (especially the minima). The differences are a bit higher here for $u_{10} = 10\,\mathrm{m/s}$ than for $u_{10} = 7\,\mathrm{m/s}$, owing to the higher contrast in the RMS slopes which implies a higher contrast in the shadowing effects. Then, as a general rule, for H polarization, the oil slick detection is easier as the wind speed increases. For V polarization, one can observe a significant difference between the clean sea surface and the sea covered in oil: the dynamics of the curves and the positions of the extrema of the curves are different. This is due to the Brewster effect, which occurs only in V polarization. Indeed, the Brewster incidence angle θ_i^B for the lossless sea surface ($\epsilon_{r3} = 70$) is $\theta_i^B \simeq 83.2°$, whereas the one for the lossless oil interface ($\epsilon_{r2} = 2.2$) is $\theta_i^B \simeq 56.0°$. Then, for the lossy media considered in equations (73) and (74), the minimum of the absolute value of the reflection coefficient occurs for an incident angle rather close to θ_i^B. As h_2 ranges from 0 to 30 m for $x_2 = 2$ km, θ_i ranges from 89.6° to 88.6°: then, the reflection coefficient r_{12} is much closer to 0 for the sea surface than for the air-oil interface, where it is close to 1. This accounts for the lower dynamics in η for the clean sea surface in comparison with the contaminated sea.

Moreover, the differences in the positions of the extrema between the clean and the contaminated sea for V polarization are mainly due to the differences in the phase of the reflection coefficient $\angle r_{12}$

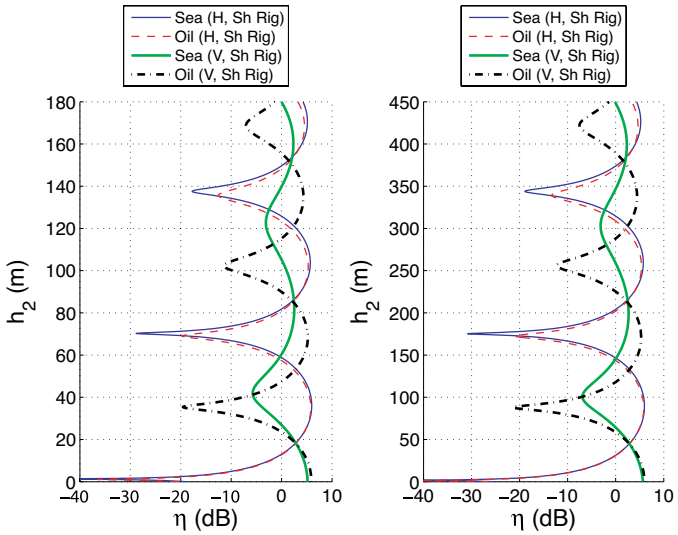

Figure 12. Comparison between a clean sea surface and a sea covered in oil for H and V polarizations, with $u_{10} = 10\,\mathrm{m/s}$ and $f = 300\,\mathrm{MHz}$.

due to the Brewster effect (they are also influenced by the shadowing effect, but more slightly). Indeed, for H polarization and $x_2 = 2$ km, $\angle r_{12} \in [0.03°; 0.08°]$ for the sea surface and $[0.00°; 0.01°]$ for the air-oil interface, whereas for V polarization, $\angle r_{12} \in [-6.95°; -2.00°]$ for the sea surface and $[-0.002°; -0.000°]$ for the air-oil interface.

Thus, the differences between the clean and the contaminated seas are much more significant for V polarization than for H polarization, allowing much easier detection of an oil slick. Fig. 12 presents the same results as Fig. 11, but for a frequency $f = 300$ MHz. Let us note that following [4–6], the results of the approximate methods are in excellent agreement with exact numerical methods. Indeed, the Ament model is valid for $R_{a,r} < 1.25$ [9], and here, for $x_2 = 2\,\mathrm{km}$, $h_2 \in [0; 180]\,\mathrm{m}$, which implies that $R_{a,r} \in [0.031; 0.402]$, and for $x_2 = 5\,\mathrm{km}$, $h_2 \in [0; 450]\,\mathrm{m}$, which implies that $R_{a,r} \in [0.012; 0.383]$. The numerical results for H polarization highlight a higher contrast between the sea and the oil for this frequency, in comparison with Fig. 11 where $f = 3\,\mathrm{GHz}$, making the oil slick detection easier. For V polarization, the phase difference of the reflection coefficient between the sea and the oil increases significantly. Then, the two curves differ significantly for any height of the receiver h_2, making the oil slick detection easy for V polarization. Thus, the oil slick detection is easier for lower radar frequencies.

6. CONCLUSION

In conclusion, the forward radar propagation over rough surfaces using the Ament model [9] has been extended to the case of rough layers, and applied to a sea covered in oil, by taking the shadowing effect into account. A comparison between a clean sea surface and a sea covered in oil has been detailed. For the typical applications (micro-wave frequencies and coastal radar configuration) presented, it is shown that only the reflection from the air/oil interface of the contaminated sea contributes to the forward radar propagation over the rough layer. Then, for H polarization, the case of a sea covered in oil significantly differs from the clean sea surface only around the extrema (and especially the minima) of the propagation factor. This contrast is increased for lower ranges x_2 and higher heights h_2 of the receiver. By contrast, for V polarization, the case of a sea covered in oil differs from the clean sea surface owing to the Brewster effect which contributes for the clean sea surface. This induces a high contrast in the positions and amplitudes of the extrema of the propagation factor, allowing to detect oil slicks easily. Moreover, the lower the frequency is, and the higher the wind speed is, the easier the detection will be.

REFERENCES

1. Hsieh, C.-Y. and A. K. Fung, "Depolarized upward and downward multiple scattering from a very rough surface," *Progress In Electromagnetics Research*, PIER 54, 199–220, 2005.
2. Fung, A. K. and N. C. Kuo, "Backscattering from multi-scale and exponentially correlated surfaces," *Journal of Electromagnetic Waves and Applications*, Vol. 20, No. 1, 3–11, 2006.
3. Chen, K. S., A. K. Fung, J. C. Shi, and H. W. Lee, "Interpretation of backscattering mechanisms form non-Gaussian correlated randomly rough surfaces," *Journal of Electromagnetic Waves and Applications*, Vol. 20, No. 1, 105–118, 2006.
4. Berginc, G. and C. Bourrely, "The small-slope approximation method applied to a three-dimensional slab with rough boundaries," *Progress In Electromagnetics Research*, PIER 73, 131–211, 2007.
5. Ament, W., "Toward a theory of reflection by a rough surface," *IRE Proc.*, Vol. 41, 142–146, 1953.
6. Fabbro, V., P. Combes, and N. Guillet, "Apparent radar cross section of a large target illuminated by a surface wave above

the sea," *Progress In Electromagnetics Research*, PIER 50, 41–60, 2005.

7. Oraizi, H. and S. Hosseinzadeh, "A novel marching algorithm for radio wave propagation modelling over rough surfaces," *Progress In Electromagnetics Research*, PIER 57, 85–100, 2006.
8. Fabbro, V., C. Bourlier, and P. Combes, "Forward propagation modeling above Gaussian rough surfaces by the parabolic wave equation: introduction of the shadowing effect," *Progress In Electromagnetics Research*, Vol. 58, 243–69, 2006.
9. Freund, D., N. Woods, H.-C. Ku, and R. Awadallah, "Forward Radar propagation over a rough sea surface: a numerical assessment of the Miller-brown approximation using a horizontally polarized 3-Ghz line source," *IEEE Transactions on Antennas and Propagation*, Vol. 54, 1292–304, Apr. 2006.
10. Pinel, N., C. Bourlier, and J. Saillard, "Rayleigh parameter of a rough layer: Application to forward radar propagation over oil slicks on sea surfaces under the Ament model," *Microwave and Optical Technology Letters*, Vol. 49, 2285–2290, Sep. 2007.
11. Ogilvy, J., *Theory of Wave Scattering from Random Surfaces*, Institute of Physics Publishing, Bristol and Philadelphia, 1991.
12. Born, M. and E. Wolf, *Principles of Optics*, 6th edition, Pergamon, London, 1980.
13. Smith, B., "Lunar surface roughness: shadowing and thermal emission," *Journal of Geophysical Research*, Vol. 72, 4059–4067, Aug. 1967.
14. Smith, B., "Geometrical shadowing of a random rough surface," *IEEE Transactions on Antennas and Propagation*, Vol. 15, 668–671, Sept. 1967.
15. Pinel, N., C. Bourlier, and J. Saillard, "Energy conservation of the scattering from rough surfaces in the high-frequency limit," *Optics Letters*, Vol. 30, 2007–2009, Aug. 2005.
16. Tsang, L. and J. Kong, *Scattering of Electromagnetic Waves*, Volume III: Advanced Topics, John Wiley & Sons, New York, 2001.
17. Abramowitz, M. and I. Stegun, *Handbook of Mathematical Functions*, Dover Publications, New York, 1972.
18. Brockelman, R. and T. Hagfors, "Note on the effect of shadowing on the backscattering of waves from a random rough surface," *IEEE Transactions on Antennas and Propagation*, Vol. 14, 621–626, Sept. 1966.
19. Bourlier, C., G. Berginc, and J. Saillard, "Monostatic and bistatic

statistical shadowing functions from a one-dimensional stationary randomly rough surface according to the observation length: I. Single scattering," *Waves in Random Media*, Vol. 12, No. 2, 145–173, 2002.

20. Ulaby, F., R. Moore, and A. Fung, *Microwave Remote Sensing: Active and passive*, Vol. 3 - From Theory to Applications. Artech House, Norwood, 1986.
21. Friizo, T., Y. Schildberg, O. Rambeau, T. Tjomsland, H. Fordedal, and J. Sjoblom, "Complex permittivity of crude oils and solutions of heavy crude oils fractions," *Journal of Dispersion Science and Technology*, Vol. 19, No. 1, 93–126, 1998.
22. Elfouhaily, T., B. Chapron, K. Katsaros, and D. Vandemark, "A unified directional spectrum for long and short wind-driven waves," *Journal of Geophysical Research*, Vol. 102, No. C7, 781–796, 1997.
23. Lombardini, P., B. Fiscella, P. Trivero, C. Cappa, and W. Garrett, "Modulation of the spectra of short gravity waves by sea surface films: slick detection and characterization with a microwave probe," *Journal of Atmospheric and Oceanic Technology*, Vol. 6, 882–890, Dec. 1989.
24. Pinel, N., N. Déchamps, and C. Bourlier, "Modeling of the bistatic electromagnetic scattering from sea surfaces covered in oil for microwave applications." Accepted in *IEEE Transactions on Geoscience and Remote Sensing*.
25. Cox, C. and W. Munk, "Measurement of the roughness of the sea surface from photographs of the sun's glitter," *Journal of the Optical Society of America*, Vol. 44, 838–850, 1954.